Molecular Precursor Mediated Facile Synthesis of Phase Pure Metal Rich Digenite (Cu$_{1.8}$S) Nanocrystals: An Efficient Anode for Lithium ion Battery

Gourab Karmakar,[a,b] Adish Tyagi,*[a,b] Kruti K. Halankar,[a] Sandeep Nigam,[a,b] B. P. Mandal,[a,b] A. P. Wadawale,[a] G. Kedarnath,*[a,b] Anil K. Debnath,[b,c]

[a]Chemistry Division, Bhabha Atomic Research Centre, Mumbai- 400 085 (India)

[b]Homi Bhabha National Institute, Anushaktinagar, Mumbai- 400 094 (India)

[c]Technical Physics Division, Bhabha Atomic Research Centre, Mumbai, 400 085 (India)

Email: tyagia@barc.gov.in, kedar@barc.gov.in

EXPERIMENTAL SECTION

Cuprous chloride (CuCl$_2$•2H$_2$O), oleylamine (OAm), 1-octadecene (ODE), trioctylphosphine oxide (TOPO), triphenyl phosphine (PPh$_3$) and analytical grade solvents were obtained from commercial sources. The ligand; 4,6-dimethyl-2-mercaptopyrimidine: (2-HSpymMe$_2$) (^{1}H NMR (D$_2$O) δ: 2.49 (s, Me); 6.94 (s, CH-5). ^{13}C{^{1}H} NMR (D$_2$O) δ: 19.6 (Me); 111.5 (CH-5); 168.0 (C-2); 173.3 (C-4,6)) was prepared according to a literature method.[1] Elemental analyses were carried out on a Thermo Fischer Flash EA1112 CHNS analyzer. The ^{1}H, ^{13}C{^{1}H} and ^{31}P{^{1}H} NMR spectra were recorded on a Bruker Advance-II NMR spectrometer operating at 300, 75.47 and 121.49 MHz, respectively. Chemical shifts are relative to internal chloroform peak for ^{1}H NMR spectra.

Thermogravimetric analyses (TGA) were carried out using a Nitzsch STA 409 PC-Luxx TG-DTA instrument that was calibrated with CaC$_2$O$_4$·H$_2$O. The TG curves were recorded at a heating rate of 10ºC min^{-1} under a flow of argon. The X-ray powder diffraction patterns were obtained using a Philips PW-1820 diffractometer using Cu-K$_\alpha$ radiation. XPS measurements were carried out using Mg-K$_\alpha$ (1253.6 eV) source and DESA-150 electron analyzer (Staib Instruments, Germany). For XPS analysis, a film was prepared by drop coating the sample on glass substrate and drying under the IR lamp. The binding energy scale in XPS was calibrated to C-1s line of 284.5 eV. All the deconvolutions and fittings were done by the CasaXPS software. Optical diffuse reflectance measurements in the range 200–1100 nm (1.12 eV to 6.2 eV) was performed using a JASCO V-670 two-beam spectrometer with a diffuse reflectance (DR) attachment consisting of an integration sphere coated with BaSO$_4$ which was

used as the reference material. The measured reflectance data were converted to absorption (A) using the Kubelka–Munk remission function.[2] The band gaps of the samples were estimated by extrapolating the linear portion of the plot to X(energy) axis. Raman spectra were recorded using the 633 nm line from a He-Ne laser. The samples were taken on glass slide and Raman scattering light was collected at back scattering geometry with a 50X LWD (long working distance) objective and detected using a CCD (Synapse) based monochromator (LabRAM HR800, Horiba Jobin Yvon, France) together with an edge filter and the accuracy of the spectral measurement was estimated to be better than 1 cm^{-1}. SEM and EDS measurements were carried out using an ULTRA 55 FESEM of Zeiss and Oxford Inca instruments, respectively. A Zeiss Libra 200 FE Transmission electron microscope (TEM) operating at an accelerating voltage of 200 kV was used for TEM studies. The samples for TEM were prepared by placing a drop of sample dispersed in acetone/toluene on a carbon coated copper grid.

The Intensity data for $[(PPh_3)_2CuCl(SpymMe_2)]$ was collected at room temperature (298 ± 2 K) using a Rigaku AFC7S diffractometer using graphite monochromated Mo-Kα (λ = 0.71069 Å) radiation so that θ_{max} = 27.5°. The unit cell parameters were determined from 25 reflections measured by a random search routine. The intensity data were corrected for Lorentz, polarization and absorption effects using an empirical procedure.[3] The structures were solved by direct methods using SHELX-2014/6[4] and refined by the full-matrix least squares methods. The non-hydrogen atoms were refined anisotropically. The hydrogen atoms were fixed in their calculated positions. Molecular structure was drawn using ORTEP.[5]

Synthesis of $[(PPh_3)_2CuCl(SpymMe_2)]$. To a freshly prepared solution of $NaSpymMe_2$ in methanol (obtained from a methanolic solutions of $2\text{-}HSpymMe_2$ (200 mg, 1.42 mmol) and CH_3ONa (7.2 mL of 0.2 M), 1.42 mmol), a solution of $CuCl_2 \cdot 2H_2O$ (242 mg, 1.42 mmol) and PPh_3 (745 mg, 2.84 mmol) in CH_3CN was slowly added with constant stirring. The solution turns bright yellow and the reaction was continued for 2 h. The solvent was removed under vacuum and the final product was extracted with dicholoromethane. The solution upon slow evaporation, resulted into bright yellow crystals of the title complex (yield: 951 mg, 87.8 %), m.p. 187°C (decomp.). Anal. Calcd. For $C_{42}H_{37}ClCuN_2P_2S$: C, 66.13; H, 4.88; N, 3.67; S, 4.20%. Observed: C, 66.02; H, 4.72; N, 3.09; S, 3.98%. ^1H NMR (CDCl$_3$) δ: 2.00 (s, $C_4H(Me\text{-}4,6)N_2$, 6 H); 6.38 (s, $CH\text{-}5$, $C_4H(Me\text{-}4,6)N_2$); 7.20-7.25 (m, 30H, $2PPh_3$). $^{31}P\{^1H\}$ NMR (CDCl$_3$) δ: -3.43 ppm.

Synthesis of copper sulfide nanostructures. Copper sulfide nanostructures were synthesized by thermolysis of $[(PPh_3)_2CuCl(SpymMe_2)]$ in different high boiling solvents employing hot injection method. Three sets of experiments were carried out to investigate the effect of the reaction conditions and solvents on the phase purity and morphology of the nanostructures. In a typical hot injection method, 8 mL of high boiling solvent (TOPO, OAm or ODE) was taken in a three-necked round bottom flask and degassed at 120°C under nitrogen flow for 30 min. Subsequently, the temperature was elevated to 250°C and required amount of the precursor $[(PPh_3)_2CuCl(SpymMe_2)]$ (500 mg, 0.65 mmol), dispersed in 2 mL of same solvent was rapidly injected. The reaction temperature dropped by around ~20°C upon injection; however, the set temperature was attained swiftly. The reaction was continued for 10 minutes while maintaining the temperature, after which the reaction mixture was allowed to cool to 60°C followed by addition of 5 mL methanol to ensure complete precipitation of the nanostructures. The synthesized material was collected after repeated washing with methanol and toluene mixture followed by centrifugation at 8000 rpm for 10 minutes to remove excess capping agent. The final product was collected as shiny black residue.

Cell fabrication and electrochemical characterization. The as-prepared copper sulfide nanocrystals was mixed with super P carbon black and the water soluble binder sodium alginate in a weight ratio of 70:20:10, respectively, to form a consistent slurry. This slurry was then uniformly coated on a clean copper foil (1 × 1 cm) which is then used as a current collector. These electrodes were then allowed to dry in a preheated oven at 50°C for about 8 h. The mass loading was controlled to be within 2.5–2.8 mg cm^{-2}. The electrochemical properties of the $Cu_{1.8}S$ electrodes were characterized by fabricating in CR2032-type coin cells. The lithium foil is used as a reference and a counter electrode. A piece of glass fibre was used as the separator, and $LiPF_6$ (1 mol L^{-1} in EC : DMC = 1 : 1 (v/v %)) was used as the electrolyte to assemble LIBs. The cells were galvanostatically charged and discharged under increasing current densities to evaluate the rate performance at different current densities. Cyclic voltammetric measurements were carried out using an electrochemical workstation (OrigaLys, France). Impedance measurement of the cells were carried out using Novocontrol Alpha A High-Frequency Analyzer. Impedance measurement was carried out an AC voltage of 10 mV in the frequency range 1 Hz–1 MHz at room temperature

Theoretical calculations. Theoretical calculations were carried out under DFT formalism. Plane wave based pseudo-potential approach as implemented in the Vienna ab initio Simulation Package (VASP)[6,7] has been utilized for all calculations. Full-potential all-electron projector augmented wave (PAW) method[8,9] has been used for electron–ion interaction representation. Exchange-correlation energy has been described by spin polarized generalized gradient approximation (GGA).[10] An energy cut-off of 400 eV and 3 x 3 x3 k-point mesh were found to be enough to converge the total ground state energy within 1 meV.

REFERENCES

1. Karmakar, G.; Tyagi, A.; Shah, A. Y.; Wadawale, A. P.; Kedarnath, G.; Singh, V. Molecular precursor driven synthesis of phase pure tin sulfide nanosheets and investigation of their photoresponsive behaviour. *Polyhedron* **2022**, *220*, 115833.

2. Philips-Invernizzi, B.; Dupont, D.; Caze, C. Bibliographical review for reflectance of diffusing media. *Opt. Eng.* **2001**, *40*, 1082–1092.

3. Higashi, T.; ABSCOR-Empirical Absorption Correction based on Fourier Series Approximation, Rigaku Corporation, 3-9-12 Matsubara, Akishima, Japan, **1995**.

4. Sheldrick, G. M. A short history of SHELX. *Acta Crystallogr., Sect. A: Found. Crystallogr.* **2008**, *64*, 112–122.

5. Johnson, C. K. ORTEP II, Report ORNL-5136, Oak Ridge National Laboratory, Oak Ridge TN, **1976**.

6. Kresse, G.; Furthmuller, J. Efficient iterative schemes for ab initio total-energy calculations using a plane-wave basis set. *Phys. Rev. B*. **1996**, *54*, 11169–11186.

7. Vanderbilt, D. Soft self-consistent pseudopotentials in generalized eigenvalue formalism. *Phys. Rev. B*. **1990**, *41*, 7892–7895.

8. Blochl, P. E. Projector augmented-wave method. *Phys. Rev. B*. **1994**, *50*, 17953–17979.

9. Kresse, G.; Joubert, J. From ultrasoft pseudopotentials to the projector augmented-wave method. *Phys. Rev. B*. **1999**, *59*, 1758–1775.

10. Perdew, J. P.; Chevary, J. A.; Vosko, S. K.; Jackson, K. A.; Pederson, M. R.; Singh, D. J.; Fiolhias, C. Atoms, molecules, solids, and surfaces: Applications of the generalized gradient approximation for exchange and correlation. *Phys. Rev. B*. **1992**, *46*, 6671–6687.

Figure Captions:

Figure S-1. $^{31}P\{^1H\}$ NMR spectra of $[(PPh_3)_2CuCl(SpymMe_2)]$.

Figure S-2. (A) unit cell and (B) crystal packing diagram of $[(PPh_3)_2CuCl(SpymMe_2)]$.

Figure S-3. pXRD pattern of TG residue obtained after thermal decomposition of $[(PPh_3)_2CuCl(SpymMe_2)]$ at 800°C.

Figure S-4. EDS spectrum of copper sulfide nanostructures obtained by the thermolysis of $[(PPh_3)_2CuCl(SpymMe_2)]$ at 250°C for 10 minutes in (a) ODE, (b) OAm and (c) TOPO respectively.

Figure S-5. FT-IR spectra of copper sulfide nanostructures obtained by the thermolysis of $[(PPh_3)_2CuCl(SpymMe_2)]$ at 250°C for 10 minutes in (a) OAm and (b) TOPO respectively.

Figure S-6. TG of copper sulfide nanostructures obtained by the thermolysis of $[(PPh_3)_2CuCl(SpymMe_2)]$ at 250°C for 10 minutes in (a) OAm and (b) TOPO respectively.

Figure S-7. 2-D elemental mapping of copper sulfide nanostructures obtained by the thermolysis of $[(PPh_3)_2CuCl(SpymMe_2)]$ at 250°C for 10 minutes in (a) ODE, (b) OAm and (c) TOPO respectively.

Figure S-8. XPS survey scan of $Cu_{1.8}S$ synthesized by thermolysis of $[(PPh_3)_2CuCl(SpymMe_2)]$ at 250°C for 10 minutes in (a) ODE, (b) OAm and (c) TOPO respectively.

Figure S-9. SAED pattern of copper sulfide nanostructures obtained by the thermolysis of $[(PPh_3)_2CuCl(SpymMe_2)]$ at 250°C for 10 minutes in (a) ODE, (b) OAm and (c) TOPO respectively.

Figure S-10. Crystal structure of Cu_2S

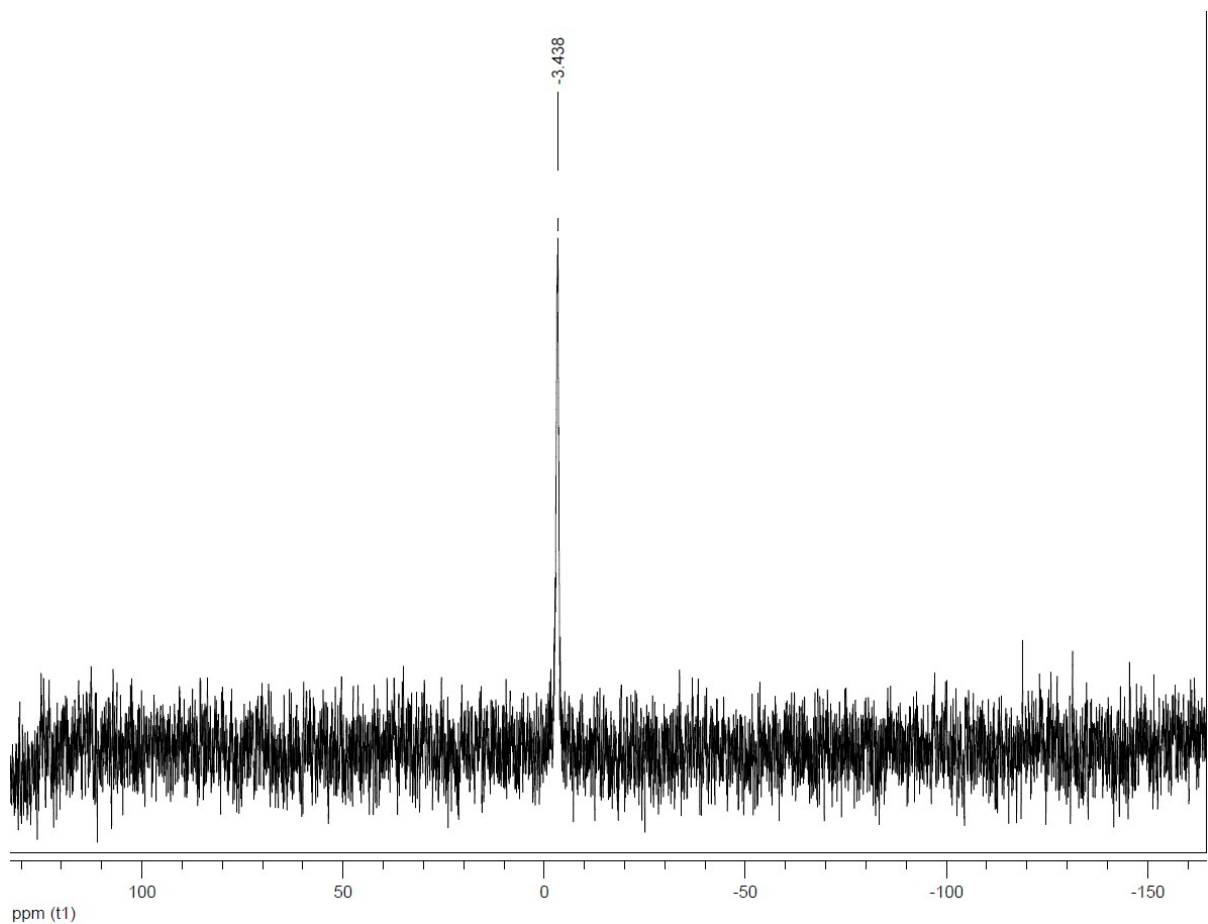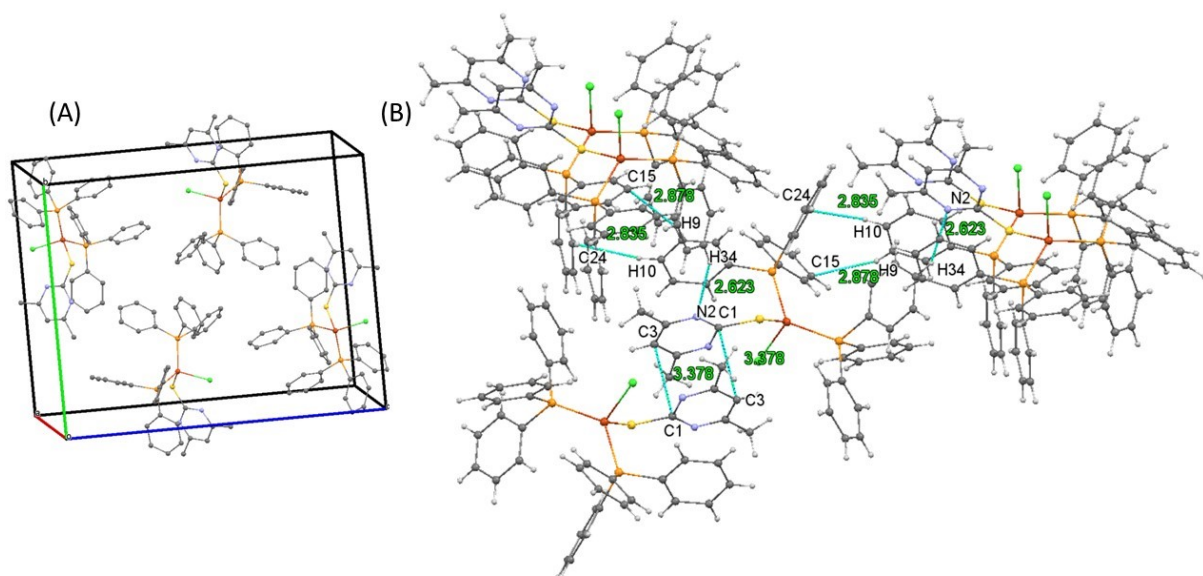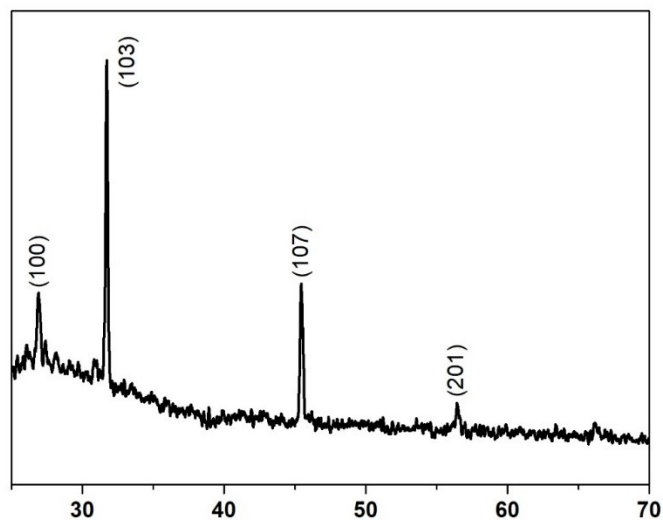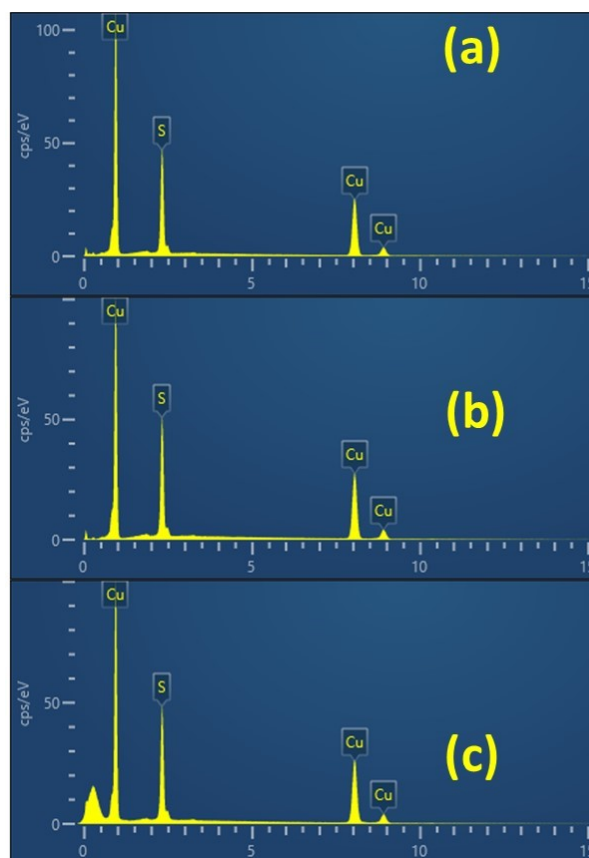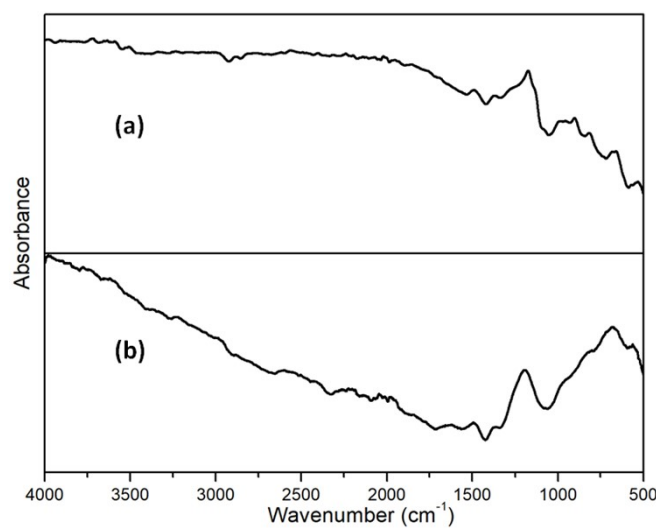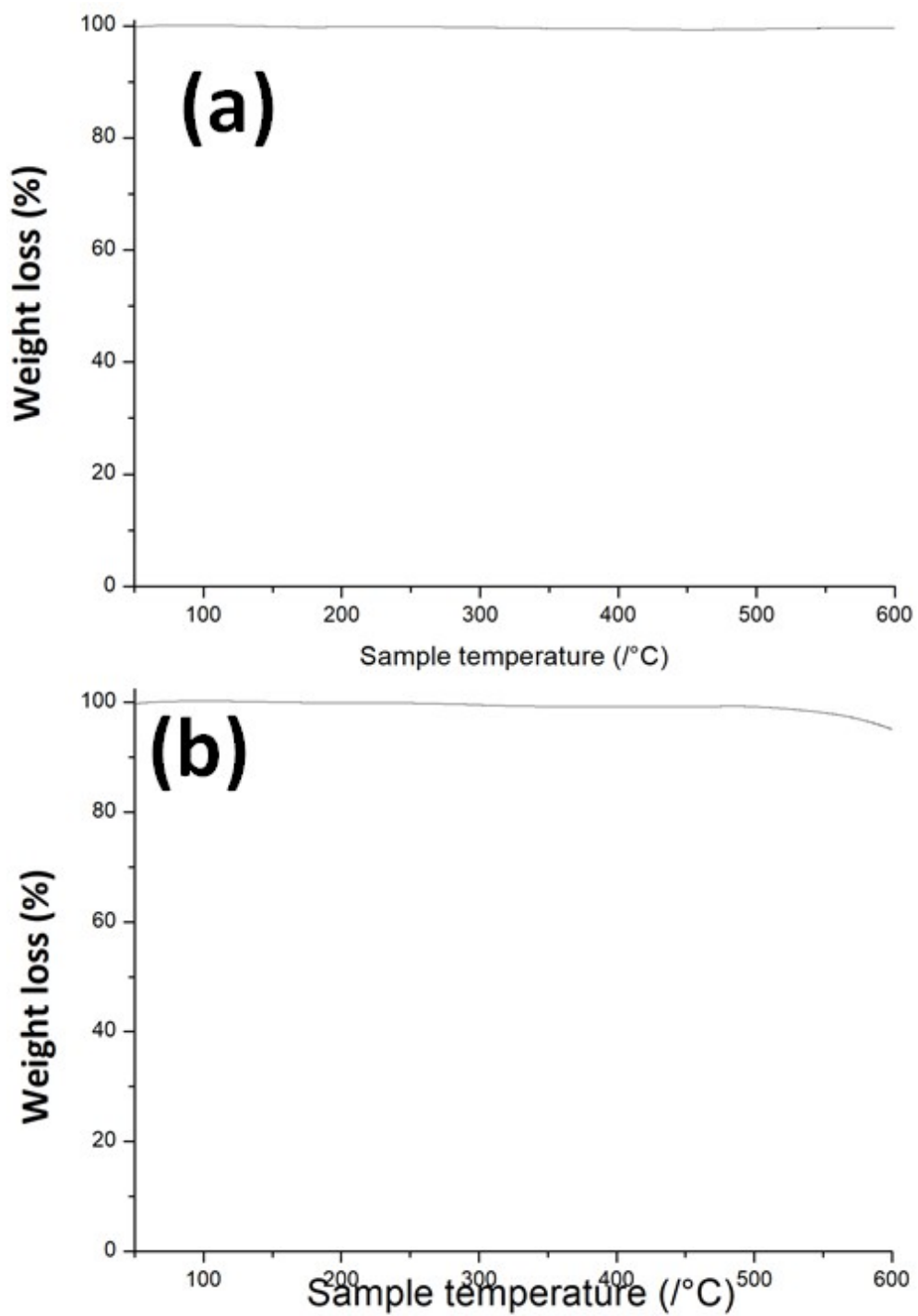**Figure S-11.** Optimized supercell of $Cu_{1.8}S$ after incorporation of Li.

Figure S-1. $^{31}P\{^1H\}$ NMR spectra of [(PPh$_3$)$_2$CuCl(SpymMe$_2$)].

Figure S-2. (A) unit cell and (B) crystal packing diagram of [(PPh$_3$)$_2$CuCl(SpymMe$_2$)].

Figure S-3. pXRD pattern of TG residue obtained after thermal decomposition of [(PPh$_3$)$_2$CuCl(SpymMe$_2$)] at 800°C.

Figure S-4. EDS spectrum of copper sulfide nanostructures obtained by the thermolysis of [(PPh$_3$)$_2$CuCl(SpymMe$_2$)] at 250°C for 10 minutes in (a) ODE, (b) OAm and (c) TOPO respectively.

Figure S-5. FT-IR spectra of copper sulfide nanostructures obtained by the thermolysis of [(PPh$_3$)$_2$CuCl(SpymMe$_2$)] at 250°C for 10 minutes in (a) OAm and (b) TOPO respectively.
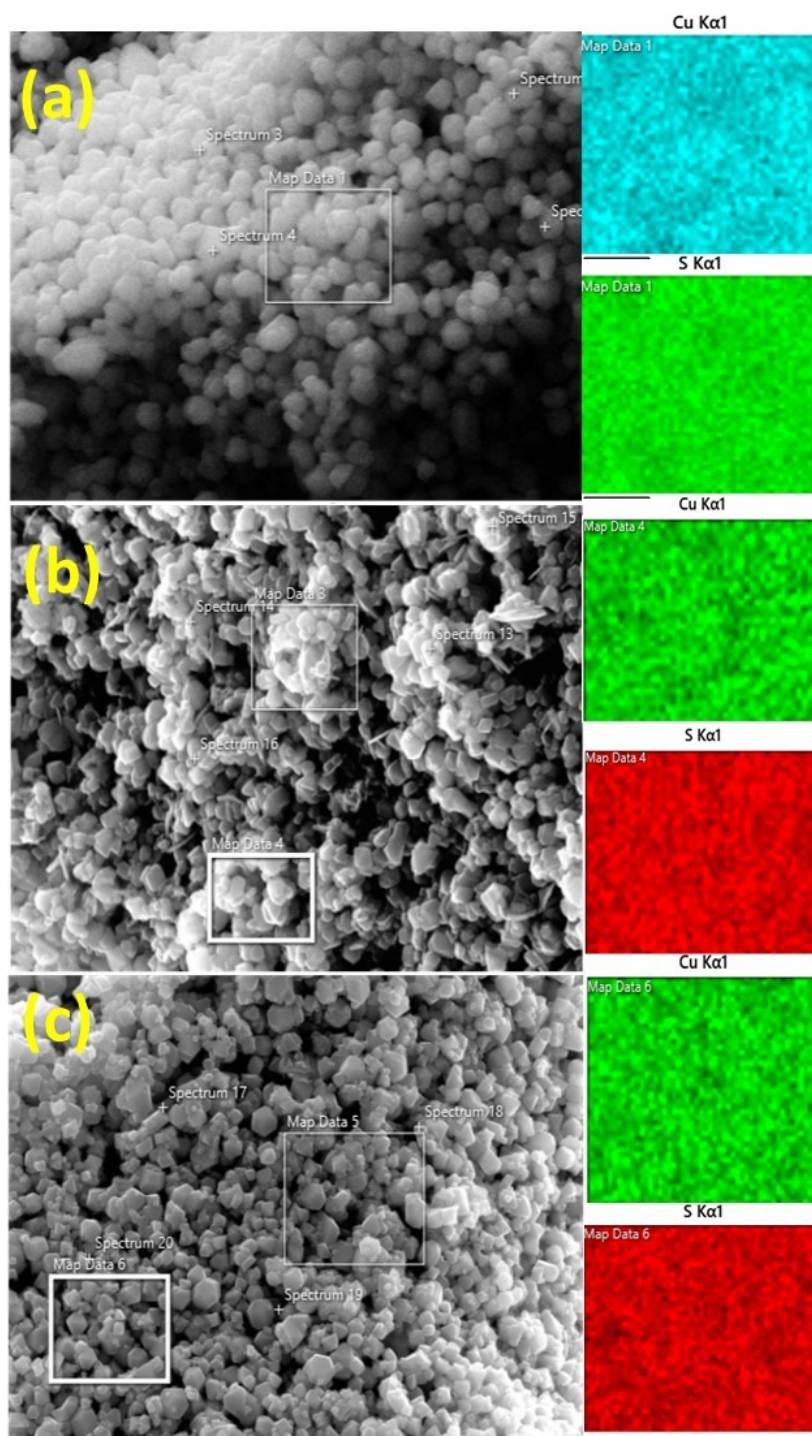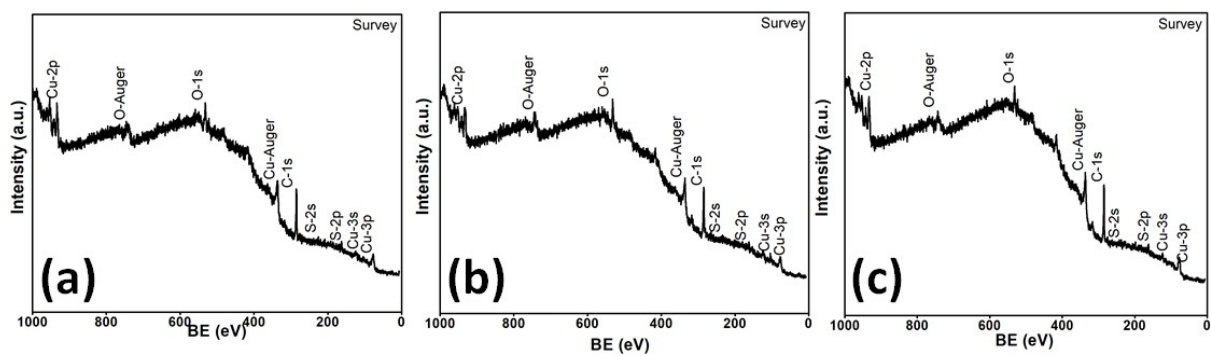
Figure S-6. TG of copper sulfide nanostructures obtained by the thermolysis of [(PPh₃)₂CuCl(SpymMe₂)] at 250°C for 10 minutes in (a) OAm and (b) TOPO respectively.

Figure S-7. 2-D elemental mapping of copper sulfide nanostructures obtained by the thermolysis of $[(PPh_3)_2CuCl(SpymMe_2)]$ at 250°C for 10 minutes in (a) ODE, (b) OAm and (c) TOPO respectively.

Figure S-8. XPS survey scan of $Cu_{1.8}S$ synthesized by thermolysis of $[(PPh_3)_2CuCl(SpymMe_2)]$ at 250°C for 10 minutes in (a) ODE, (b) OAm and (c) TOPO respectively.
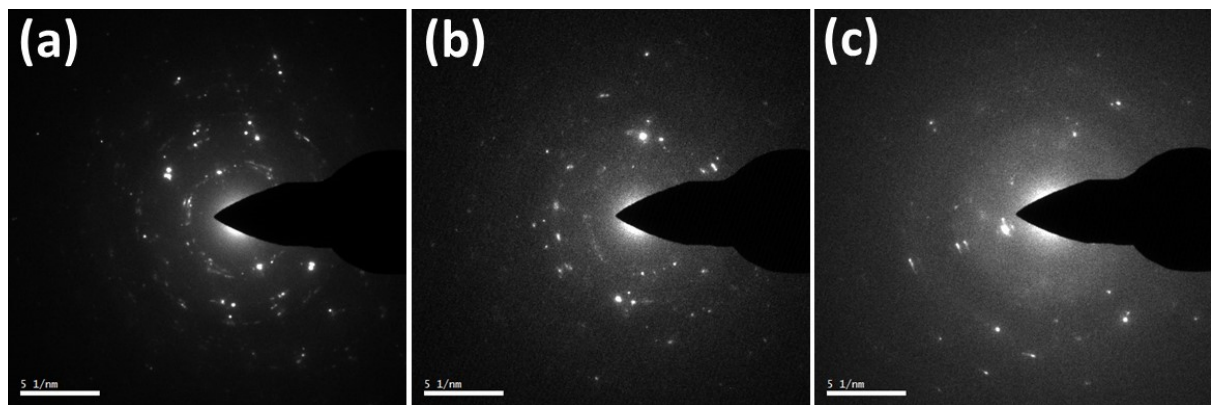

Figure S-9. SAED pattern of copper sulfide nanostructures obtained by the thermolysis of $[(PPh_3)_2CuCl(SpymMe_2)]$ at 250°C for 10 minutes in (a) ODE, (b) OAm and (c) TOPO respectively.
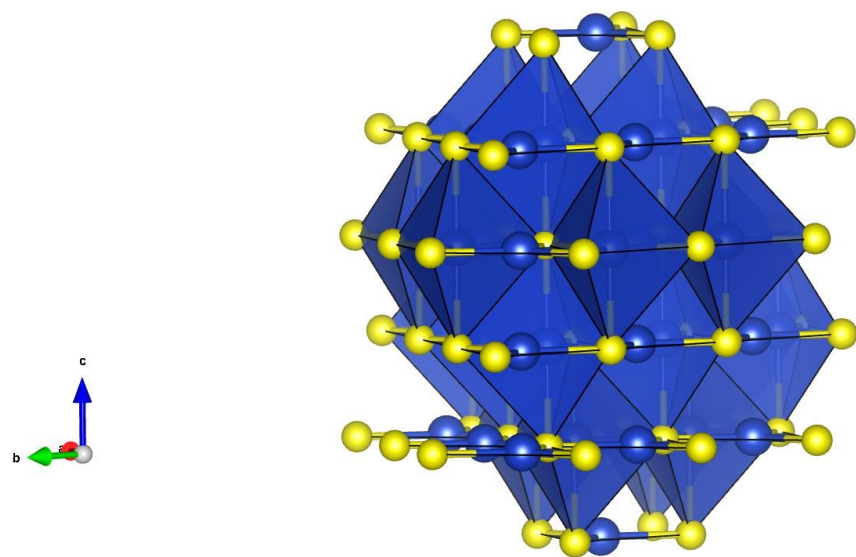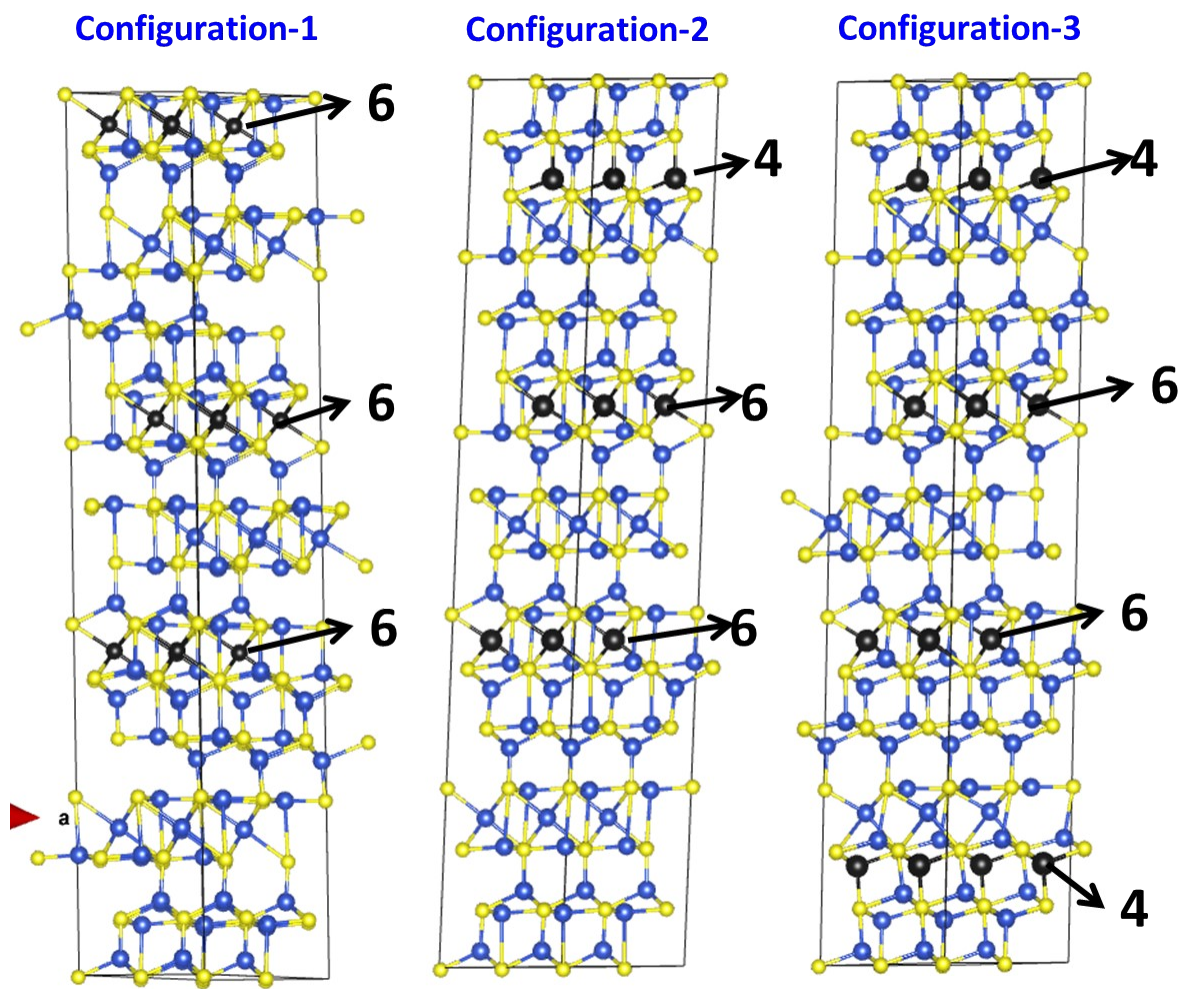
Figure S-10. Crystal structure of Cu$_2$S

Configuration-1 **Configuration-2** **Configuration-3**

Figure S-11. Optimized supercell of Cu$_{1.8}$S after incorporation of Li.